MIT–CTP–3136
SLAC–PUB–8829
hep-ph/yymmnnn

Selectron Studies at e^-e^- and e^+e^- Colliders*

Jonathan L. Feng[a†] and Michael E. Peskin[b‡]

[a] *Center for Theoretical Physics, Massachusetts Institute of Technology*
Cambridge, MA 02139 USA

[b] *Stanford Linear Accelerator Center, Stanford University*
Stanford, CA 94309 USA

Abstract

Selectrons may be studied in both e^-e^- and e^+e^- collisions at future linear colliders. Relative to e^+e^-, the e^-e^- mode benefits from negligible backgrounds and β threshold behavior for identical selectron pair production, but suffers from luminosity degradation and increased initial state radiation and beamstrahlung. We include all of these effects and compare the potential for selectron mass measurements in the two modes. The virtues of the e^-e^- collider far outweigh its disadvantages. In particular, the selectron mass may be measured to 100 MeV with a *total* integrated luminosity of 1 fb^{-1}, while more than 100 fb^{-1} is required in e^+e^- collisions for similar precision.

*Work supported by the U. S. Department of Energy, contract DE–AC03–76SF00515 and in part by the U. S. Department of Energy under cooperative research agreement DF–FC02–94ER40818.

†E-mail: jlf@mit.edu

‡E-mail: mpeskin@slac.stanford.edu

I. INTRODUCTION

If new particles exist at the weak scale, linear colliders are likely to play an important role in determining their properties and illuminating their relationships to electroweak symmetry breaking. This is especially true for supersymmetric particles. In e^+e^- collisions, linear colliders produce superpartners democratically, and the ability to specify the initial partons' energies and (in the case of electrons) spins makes possible a rich program of highly model-independent measurements [1].

The flexibility of the linear collider program is further enhanced by the possibility of e^-e^-, $e^-\gamma$, and $\gamma\gamma$ collisions. The e^-e^- possibility is a prerequisite for the $e^-\gamma$ and $\gamma\gamma$ modes, as highly polarized beams are required to produce high energy back-scattered photons. The e^-e^- mode is also an inexpensive and technologically trivial extension, and provides an ideal environment for studying beam polarization, certain precision electroweak observables, and a variety of exotic new physics possibilities. Studies of these and other topics may be found in Refs. [2–4].

In the case of supersymmetry, electric charge and lepton number conservation imply that, in simple models, only selectrons are readily produced in e^-e^- mode [5]. However, these same symmetries also eliminate many potential backgrounds to selectron events. In addition, the unique quantum numbers of the e^-e^- initial state imply that threshold cross sections for identical selectron pair production are proportional to β, the velocity of the produced selectrons. They therefore rise much more sharply than in e^+e^- collisions, where the threshold cross section is proportional to β^3. For these and other reasons to be described below, the e^-e^- mode provides a promising environment for studies of selectrons, and sleptons in general [6,7]. The potential of e^-e^- colliders for high precision studies of slepton flavor [8] and CP violation [9] and super-oblique parameters [10,11] has been considered previously.

Here we explore the potential of e^-e^- collisions for selectron threshold mass measurements. Precise measurements of superparticle masses are required to determine the parameters of the weak-scale supersymmetric Lagrangian and, ultimately, the underlying theory at shorter length scales [12]. Threshold scans have great potential, but are sensitive to beam luminosity profiles. We consider realistic beam designs as recently implemented in the `pandora` simulation package [13]. These include the effects of initial state radiation (ISR), beamstrahlung, beam energy spread, and the luminosity reduction appropriate for e^-e^- collisions. While all of these effects degrade the results, they are more than compensated for by the intrinsic benefits of e^-e^- collisions. We show, in particular, that selectron mass measurements at the part per mil level may be achieved with a total integrated luminosity of $L_{\rm tot} = 1$ fb^{-1}. In contrast, for the e^+e^- mode, we find that, even ignoring possibly large backgrounds, similar precision requires well over 100 fb^{-1}. Our e^+e^- results are roughly similar to those of previous studies [14,15], although differing quantitatively. The e^-e^- mode therefore provides incomparable opportunities for high precision selectron mass measurements with very little investment of luminosity.

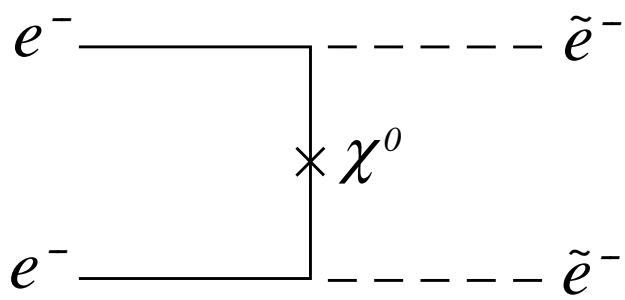

FIG. 1. Selectron pair production $e^-e^- \to \tilde{e}^-\tilde{e}^-$, mediated by t-channel neutralino exchange.

II. SELECTRON PRODUCTION AND DECAY

Selectron pair production at e^-e^- colliders takes place through the processes shown in Fig. 1. In general, each final state selectron may be either $\tilde{e}_R^-$ or $\tilde{e}_L^-$, and all four neutralinos χ_i^0 are exchanged in the t-channel. General characteristics of this production mechanism are discussed in Ref. [16].

In this study, we focus on the case of $\tilde{e}_R^-$ pair production. Right-handed sleptons are neutral under both SU(3) and SU(2) interactions. In many supersymmetric models, they are therefore the lightest scalars and so the most likely to be within kinematic reach of linear colliders. For $e^-e^- \to \tilde{e}_R^-\tilde{e}_R^-$, only t-channel Bino exchange contributes. For simplicity, we will assume that the lightest neutralino χ is a pure Bino with mass $m_\chi = M_1$, and we neglect the possibility of slepton flavor violation. (These assumptions may be tested experimentally at a linear collider, as we discuss Sec. VI.) The production cross section for $e^-e^- \to \tilde{e}_R^-\tilde{e}_R^-$, then, depends on only two supersymmetry parameters, $m_{\tilde{e}_R}$ and M_1. The differential cross section is

$$\frac{d\sigma}{d\Omega} = \frac{\alpha^2 M_1^2}{2\cos^4\theta_W}\left(\frac{1}{t-M_1^2}+\frac{1}{u-M_1^2}\right)^2 , \tag{1}$$

where the factor M_1^2 in the numerator arises from the Majorana mass insertion required in the Bino propagator.

In the reaction $e^-e^- \to \tilde{e}_R^-\tilde{e}_R^-$, the initial state of two right-handed electrons has angular momentum $L_z = 0$. The selectrons may then be produced in an S wave state, and so at threshold the cross section rises as β, the velocity of the outgoing selectrons. This contrasts sharply with the behavior of $e^+e^- \to \tilde{e}_R^+\tilde{e}_R^-$. In that reaction, the initial state is a right-handed electron and a left-handed positron, and so has $L_z = 1$. Selectrons are then necessarily produced in a P wave state, and the cross section rises as β^3 at threshold. This conclusion is based solely on the properties of the initial and final states and is independent of the relative importance of the t- and s-channel contributions to $e^+e^- \to \tilde{e}_R^+\tilde{e}_R^-$.

Once produced, selectrons must decay. In supergravity frameworks, they typically decay via $\tilde{e}_R^- \to e^-\chi$. For a Bino χ, the width is

$$\Gamma_{\tilde{e}_R} = \frac{\alpha m_{\tilde{e}_R}}{2\cos^2\theta_W}\left[1-\left(\frac{m_\chi}{m_{\tilde{e}_R}}\right)^2\right]^2 . \tag{2}$$

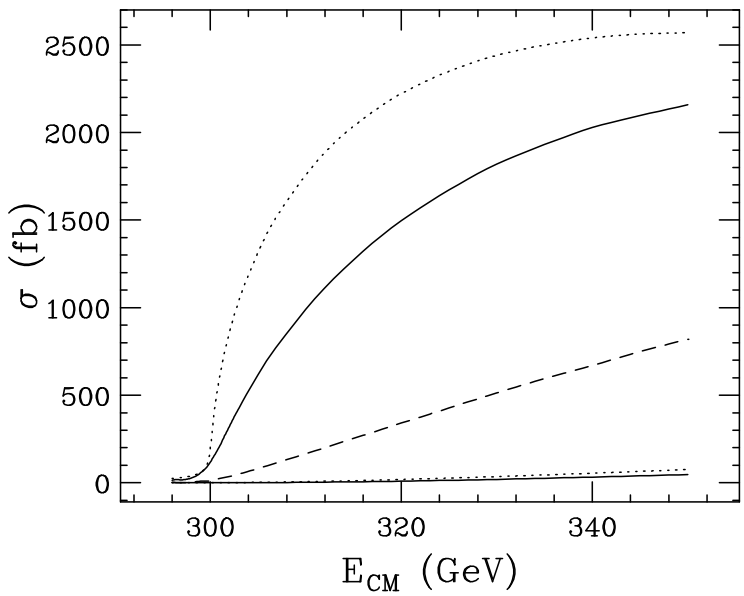

FIG. 2. Threshold behavior for $\sigma(e^-e^- \to \tilde{e}_R^-\tilde{e}_R^-)$ (upper two contours) and $\sigma(e^+e^- \to \tilde{e}_R^+\tilde{e}_R^-)$ (lower two contours) for $(m_{\tilde{e}_R}, m_\chi) = (150\text{ GeV}, 100\text{ GeV})$. In each pair, the dotted curve neglects all beam effects, and the solid curve includes the ISR/beamstrahlung and beam energy spread of the NLC500H flat beam design. Results for e^-e^- EE500 round beams (dashed) are also shown. Beam polarizations $P_{e^-} = 0.8$ and $P_{e^+} = 0$ are assumed, and the selectron width is included.

TABLE I. Beam designs considered here.

	Type	Mode	$\mathcal{L}$(300 GeV) (fb^{-1}/yr)
NLC500H [23]	flat	e^-e^-	78
NLC500H [23]	flat	e^+e^-	240
EE500 [26]	round	e^-e^-	44

In R-parity violating theories, selectrons may decay to three standard model particles, and in theories with low-energy supersymmetry breaking, selectrons may decay to gravitinos or through three-body modes to staus. If any of these is the dominant decay mode, the selectron width is negligible for calculations of threshold cross sections.

The threshold behavior of selectron production is shown in Fig. 2 for the case $(m_{\tilde{e}_R}, m_\chi) = (150\text{ GeV}, 100\text{ GeV})$ for both e^-e^- and e^+e^- modes and the beam designs given in Table I. We assume beam polarizations $P_{e^-} = 0.8$ and $P_{e^+} = 0$, where

$$P \equiv \frac{N_R - N_L}{N_R + N_L} \ . \tag{3}$$

Our treatment of the beams includes the effects of initial state radiation, beamstrahlung, and beam energy spread using approximate parameterizations which treat the two beams independently. For ISR, we use the structure function prescription, with the form of the structure function suggested by Skrzypek and Jadach [17]. For beamstrahlung, we generate the spectrum from an approximate integral equation [18] which improves upon the treatment of Yokoya and Chen [19]. This procedure makes use of phenomenological parameterizations of beam disruption at the collision due to Chen [20,21] for e^+e^- and to Chen and Thompson [22,23] for e^-e^-. For beam energy spread, we take a flat distribution with a full width

of 1% [24].

The beamstrahlung calculation requires a set of accelerator parameters. For e^+e^-, we have used the NLC high-luminosity parameter set NLC500H [25]. For e^-e^-, we have used the same parameter set modified for higher e^-e^- luminosity as suggested by Thompson [23]. The NLC500H design uses flat beams. We have also considered an earlier e^-e^- parameter set with round beams [26], which we call EE500. In addition, we have carried out our analysis for the alternative NLC parameter sets NLC500A,B,C. These give threshold cross section shapes almost identical to those with NLC500H. The luminosities for these designs are about a factor 3 smaller.

The theoretical cross sections before inclusion of beam effects are given by the dotted contours in Fig. 2. In accord with the angular momentum arguments above, the e^-e^- cross section rises rapidly at threshold. In contrast, the e^+e^- cross section rises extremely slowly. Of course, these threshold behaviors are modified after beam effects are included, as seen in the solid contours. For flat beams, however, the advantage of e^-e^- beams is preserved. For example, 10 GeV above threshold, the e^-e^- cross section is 990 fb, while the e^+e^- cross section is 2.7 fb. Note that the advantage of the e^-e^- mode is compromised for round beams — flat e^-e^- beams are essential to preserve the benefits of the β threshold behavior of $e^-e^- \to \tilde{e}_R^-\tilde{e}_R^-$.

The importance of various beam effects on the e^-e^- threshold behavior is illustrated in Figs. 3 and 4. ISR and beamstrahlung are clearly the dominant effects, significantly softening the threshold behavior in all cases. Beam energy spread also smoothes out the threshold behavior, most noticeably when the selectron width is negligible and the cross section would rise sharply at threshold otherwise. Nevertheless, even after including all beam effects, the e^-e^- cross section rises rapidly at threshold, and extremely precise measurements are possible, as we will see below.

III. SIGNAL AND BACKGROUNDS

In supergravity models, which we will focus on here, the selectron signal is $e^-e^- \to \tilde{e}_R^-\tilde{e}_R^- \to e^-e^-\chi\chi$. The signal is two like-sign electrons, each with energy bounded by

$$E_e^{\rm max}_{\rm min} = \frac{1}{2}E_b\left[1-\frac{m_\chi^2}{m_{\tilde{e}_R}^2}\right]\left[1\pm\left(1-\frac{m_{\tilde{e}_R}^2}{E_b^2}\right)^{1/2}\right] , \tag{4}$$

where E_b is the beam energy. At threshold, the electron spectrum is mono-energetic. The electrons are emitted isotropically with large p_T and $\sum p_T \neq 0$.

There are several potential backgrounds to such events, but they may all be suppressed to negligible levels with little effect on the signal. Møller scattering may be eliminated by a mild acoplanarity cut. Møller scattering with single or double bremsstrahlung may be eliminated by requiring non-vanishing $\sum p_T$ without visible photons in the event. W boson pair production, a troublesome background to selectron pair production in e^+e^- collisions, is completely eliminated by total lepton number conservation, as is chargino pair production, even if kinematically allowed. The two photon process $\gamma\gamma \to W^+W^-$, another troublesome background in e^+e^- collisions, does not produce like-sign electrons. The three-body final state e^-e^-Z, followed by $Z \to \nu\bar{\nu}$, is a possible background. However, the sum of the two

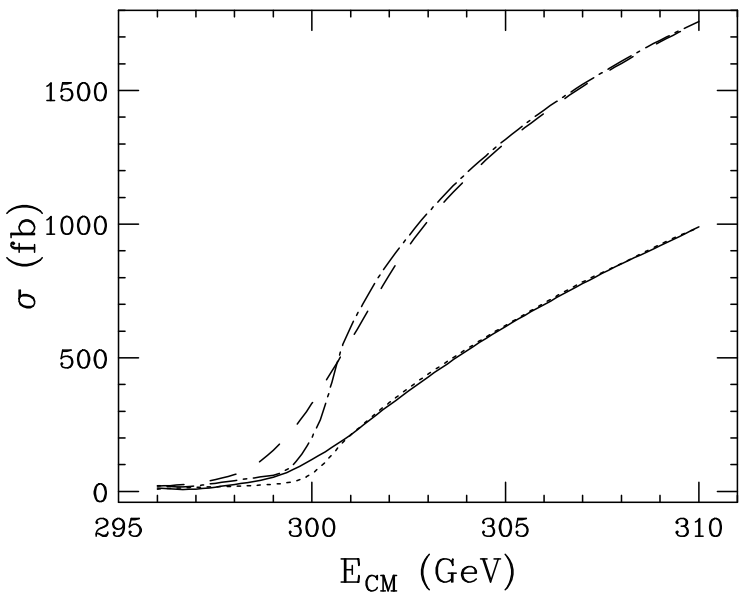

FIG. 3. Threshold behavior for $\sigma(e^-e^- \to \tilde{e}_R^-\tilde{e}_R^-)$ and $(m_{\tilde{e}_R}, m_\chi) = (150\text{ GeV}, 100\text{ GeV})$ with no beam effects (dot-dashed), only ISR/beamstrahlung (dotted), only beam energy spread (dashed), and both ISR/beamstrahlung and beam energy spread (solid). $P_{e^-} = 0.8$, and the selectron width of Eq. (2) is assumed.

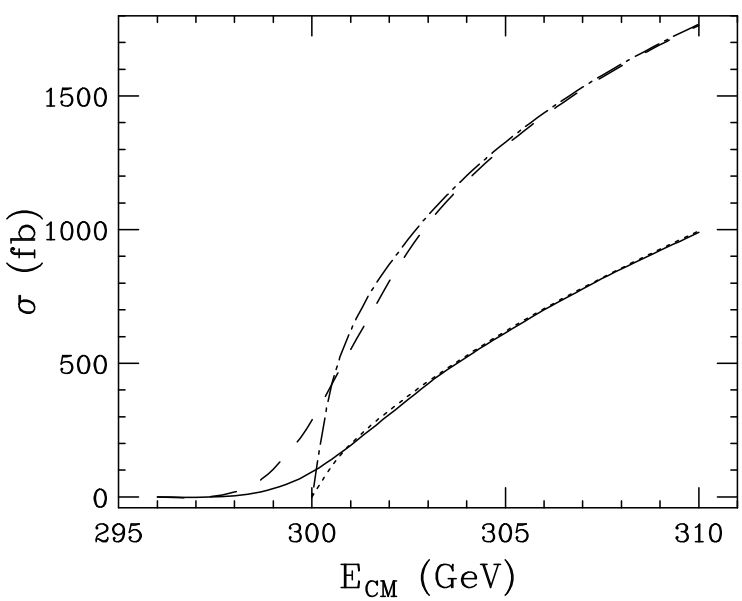

FIG. 4. As in Fig. 3, but for $\Gamma_{\tilde{e}_R} \approx 0$.

electron energies in these events is greater than $E_b[1-m_Z^2/(4E_b^2)]$. For many supersymmetry parameters, including those considered here, this constraint is inconsistent with Eq. (4), and so this background is essentially eliminated by cuts on the electron energies [27]. The background $e^-\nu W^-$, followed by $W^- \to e^-\bar{\nu}$ may be suppressed by right-polarizing *both* beams. Finally, the four-body standard model backgrounds $\nu\nu W^-W^-$ and $e^-\nu W^-Z$ [28] and the three-body supersymmetric backgrounds, such as $e^-\tilde{\nu}\tilde{W}^-$ and $e^-\tilde{e}\tilde{B}$, all have cross sections of order 1 fb or less (and in some cases may also be highly suppressed by beam polarization).

In the end, the dominant background arises from imperfect right-handed beam polarization leading to $e^-\nu W^-$. Requiring only that both electrons have pseudo-rapidity $\eta_{e^-} < 3$ ($5.7^\circ < \theta_{e^-} < 174.3^\circ$) and energy $E_{e^-} > 10$ GeV, the total background is $B \approx 110\ \text{fb} \cdot \frac{1}{4}(1-P_{e^-})^2 + 22\ \text{fb} \cdot \frac{1}{2}(1-P_{e^-}^2)$ at center-of-mass energy $E_{\rm CM} = 300$ GeV [29]. For $P_{e^-} = 0.8$ (0.9), the background is $B \approx 5.1$ fb (2.4 fb). Requiring further that both electron energies be within the range given by Eq. (4) will reduce the background to well below the fb level. The resulting background is completely negligible in e^-e^- mode, where the signal cross section quickly rises to hundreds of fb, and cross section measurements at the 1 fb level are unnecessary for high precision selectron mass measurements.

In addition to the uncertainty in background under the threshold signal, there is systematic uncertainty associated with the actual knowledge of the machine energy calibration. Not only must the beam energy be known, but also the differential luminosity spectrum must be measured to predict the cross section shape in the threshold region. Fortunately, Wilson has studied these issues in some detail for the more challenging application of measuring the W mass to 6 MeV with a scan of the W^+W^- threshold [30]. The beam energy can be determined to a few MeV with an energy spectrometer, as has been done at SLC and LEP2. The differential luminosity spectrum can be determined from the acollinearity of Bhabha events in the detector endcaps, and from $e^+e^- \to Z\gamma$ events in which a forward Z decays to leptons. Scaling down from the 100 fb^{-1} proposed by Wilson to 1 fb^{-1}, there are still ample statistics in these channels to reduce the systematic error to much less than 100 MeV.

IV. MASS DETERMINATION

We now estimate the precision of the selectron mass measurement. We consider the case $(m_{\tilde{e}_R}, m_\chi) = (150\ \text{GeV}, 100\ \text{GeV})$. The threshold behavior for these parameters, as well as the 1σ statistical error corresponding to 1 fb^{-1} at each of seven possible scan points, is shown in Fig. 5. We assume $P_{e^-} = 0.8$. In addition to suppressing background as discussed in Sec. III, this beam polarization increases the signal cross section by $(1+P_{e^-})^2 = 3.24$ relative to the unpolarized beam case.

The threshold curves for deviations $\Delta m_{\tilde{e}_R} = \pm 100$ MeV from the central value are also shown in Fig. 5. Clearly, even with 1 fb^{-1} of luminosity, deviations in $m_{\tilde{e}_R}$ of order 100 MeV may be distinguished. Note that for a fixed luminosity budget, the most stringent constraint on $m_{\tilde{e}_R}$ is achieved at $E_{\rm CM} \approx 2m_{\tilde{e}_R}$.

The identical plot, but for deviations $\Delta m_\chi = \pm 10$ GeV, is given in Fig. 6. For 1 fb^{-1}, deviations in m_χ of order 10 GeV are easily distinguished. For this purpose, however, measurements at $E_{\rm CM} \approx 2m_{\tilde{e}_R}$ are useless, and the most incisive constraint is obtained at

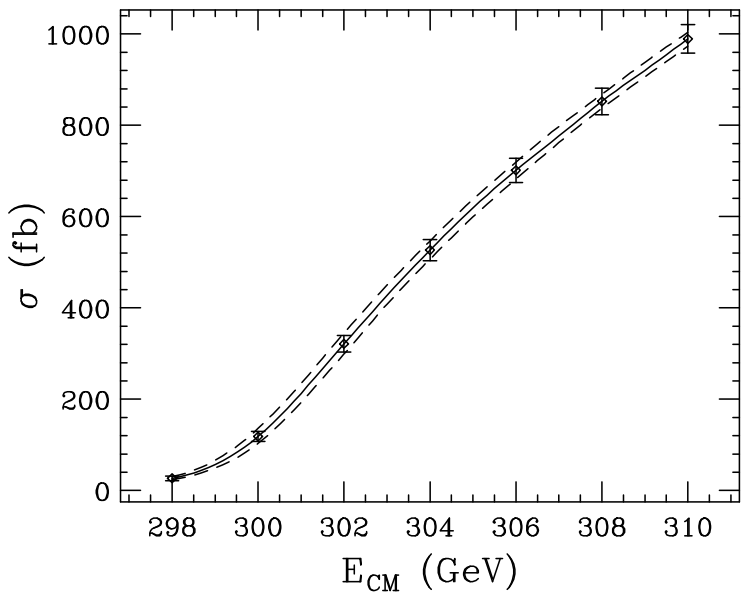

FIG. 5. Threshold behavior for $\sigma(e^-e^- \to \tilde{e}_R^-\tilde{e}_R^-)$ for $(m_{\tilde{e}_R}, m_\chi) = (150\text{ GeV}, 100\text{ GeV})$ (solid) and for $\Delta m_{\tilde{e}_R} = \pm 100$ MeV (dashed). The error bars give the 1σ statistical error corresponding to 1 fb^{-1} per point. $P_{e^-} = 0.8$, and ISR/beamstrahlung, beam energy spread, and the selectron width are included.

energies 10 to 20 GeV above threshold. This is easily understood. Larger m_χ implies larger cross sections for $E_{\rm CM} > 2m_{\tilde{e}_R}$, as a result of the Majorana mass insertion in Eq. (1), and lower cross sections for $E_{\rm CM} < 2m_{\tilde{e}_R}$, as a result of the decreased width of Eq. (2). These effects cancel at $2m_{\tilde{e}_R}$, and so the cross section there is highly insensitive to m_χ. Note also that, roughly speaking, deviations in $m_{\tilde{e}_R}$ change the normalization of the threshold curve, while deviations in m_χ change the slope. These two effects may therefore be disentangled with data taken at two or more scan points.

To determine the precision with which $m_{\tilde{e}_R}$ and M_1 may be constrained in a threshold scan, we use the binned likelihood method. We define

$$\ln \mathcal{L}(m_{\tilde{e}_R}, M_1) \equiv \sum_i N_i' \ln N_i(m_{\tilde{e}_R}, M_1) - N_i(m_{\tilde{e}_R}, M_1) \ , \tag{5}$$

where the sum is over scan points. N_i' is the measured number of events at scan point i, which we take to be the theoretical prediction given the underlying physical parameters, and $N_i(m_{\tilde{e}_R}, M_1)$ is the predicted number of events given hypothetical parameters $m_{\tilde{e}_R}$ and M_1. The parameter $\ln \mathcal{L}$ is maximized for the true underlying values of the parameters, and the width of the $\ln \mathcal{L}$ peak determines the precision with which these parameters are measured, with $\chi^2 \equiv 2(\ln \mathcal{L}_{\rm max} - \ln \mathcal{L})$ the squared standard deviation.

The optimal scan strategy depends crucially on what information is known beforehand from other processes and which parameter one most hopes to constrain. These are complicated issues. Here we consider two possibilities. First, to constrain both parameters, one might split the luminosity evenly between $E_{\rm CM} = 2m_{\tilde{e}_R}$ and $2m_{\tilde{e}_R} + 10$ GeV in a '2-point scan.' χ^2 contours in the $(m_{\tilde{e}_R}, M_1)$ plane are given in Fig. 7. For a total integrated luminosity $L_{\rm tot} = 10$ fb^{-1}, the 90% C.L. ($\chi^2 = 4.61$) ellipse (not shown) is bounded by $m_{\tilde{e}_R} = 150 \pm 0.065$ GeV and $M_1 = 100^{+5}_{-4}$ GeV. The neutralino mass is poorly constrained

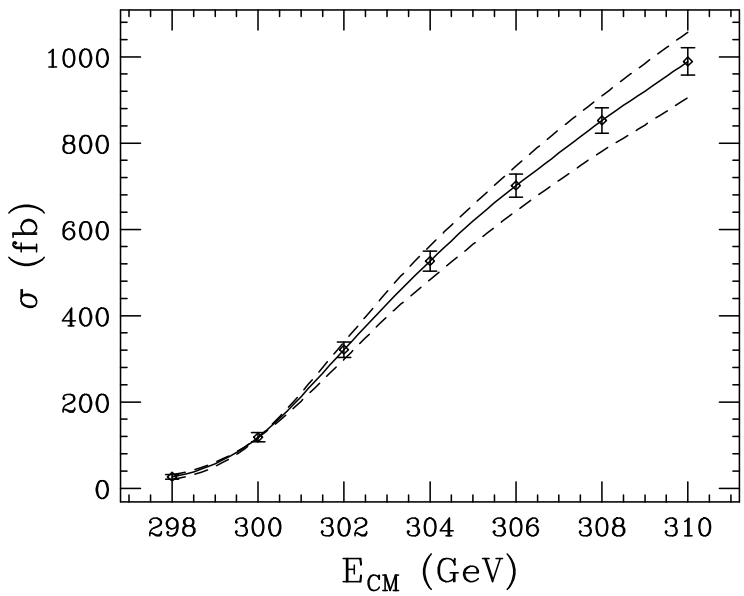

FIG. 6. Threshold behavior for $\sigma(e^-e^- \to \tilde{e}_R^-\tilde{e}_R^-)$ for $(m_{\tilde{e}_R}, m_\chi) = (150\text{ GeV}, 100\text{ GeV})$ (solid) and for $\Delta m_\chi = \pm 10$ GeV (dashed). The error bars give the 1σ statistical error corresponding to 1 fb^{-1} per point. $P_{e^-} = 0.8$, and ISR/beamstrahlung, beam energy spread, and the selectron width are included.

this way, and is likely to be determined more precisely through kinematic endpoints. In this case, projecting the $\chi^2 = 1$ ellipse down to the $m_{\tilde{e}_R}$ axis gives

$$\text{2-point scan: } L_{\rm tot}^{e^-e^-} = 1\ (10)\ \text{fb}^{-1} \Longrightarrow \Delta m_{\tilde{e}_R} = 90\ (30)\ \text{MeV}\ (1\sigma)\ . \tag{6}$$

On the other hand, given that the neutralino mass is likely to be better measured by other methods, one might simple desire to constrain the selectron mass. The optimal strategy is then to concentrate all of the luminosity at $E_{\rm CM} = 2m_{\tilde{e}_R}$, where the sensitivity to $m_{\tilde{e}_R}$ is greatest. Results of this '$m_{\tilde{e}_R}$-optimized scan' are given in Fig. 8. As expected, the neutralino mass is completely unconstrained. However, given some modest constraints on the neutralino mass from some other source, we find

$$m_{\tilde{e}_R}\text{-optimized scan: } L_{\rm tot}^{e^-e^-} = 1\ (10)\ \text{fb}^{-1} \Longrightarrow \Delta m_{\tilde{e}_R} = 70\ (20)\ \text{MeV}\ (1\sigma)\ . \tag{7}$$

Selectron mass measurements below the part per mil level are therefore possible with meager investments of luminosity.

V. COMPARISON WITH e^+e^- MODE

We now compare the results of the previous section with what can be achieved in e^+e^- collisions. The cross section $\sigma(e^+e^- \to \tilde{e}_R^+\tilde{e}_R^-)$ rises as β^3 at threshold. Values of $\mathcal{O}(1)$ fb are therefore typical even ~ 10 GeV above threshold. In addition, backgrounds such as $e^+e^- \to W^+W^-, e^-\nu W^+$ and $\gamma\gamma \to W^+W^-$ are large and difficult to eliminate. This contrasts sharply with the e^-e^- case, where the signal is large, and the analogues of these backgrounds are absent or easily suppressed. Detailed studies of these and other backgrounds, as well as

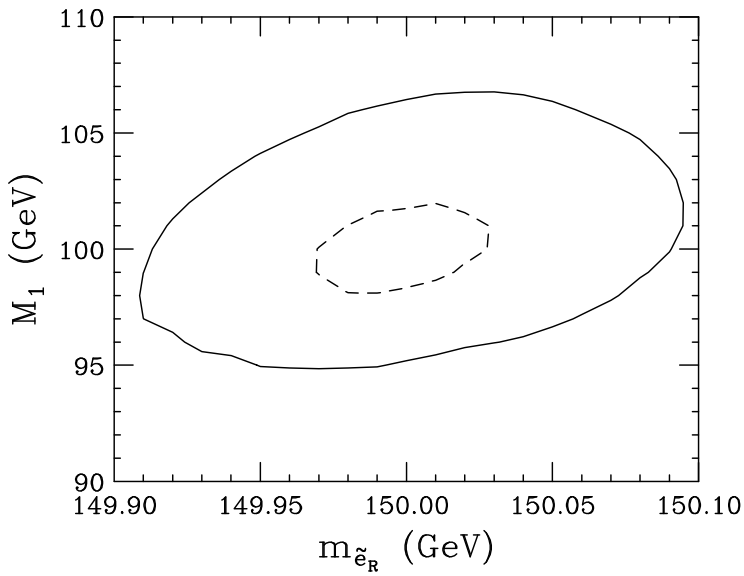

FIG. 7. $\chi^2 = 1$ constraint contours in the $(m_{\tilde{e}_R}, M_1)$ plane for the '2-point scan' of $\sigma(e^-e^- \to \tilde{e}_R^-\tilde{e}_R^-)$ for $L_{\rm tot} = 1$ fb^{-1} (solid) and 10 fb^{-1} (dashed). The luminosity is divided equally between $E_{\rm CM} = 300$ GeV and 310 GeV. $P_{e^-} = 0.8$, and ISR/beamstrahlung, beam energy spread, and the selectron width of Eq. (2) are included.

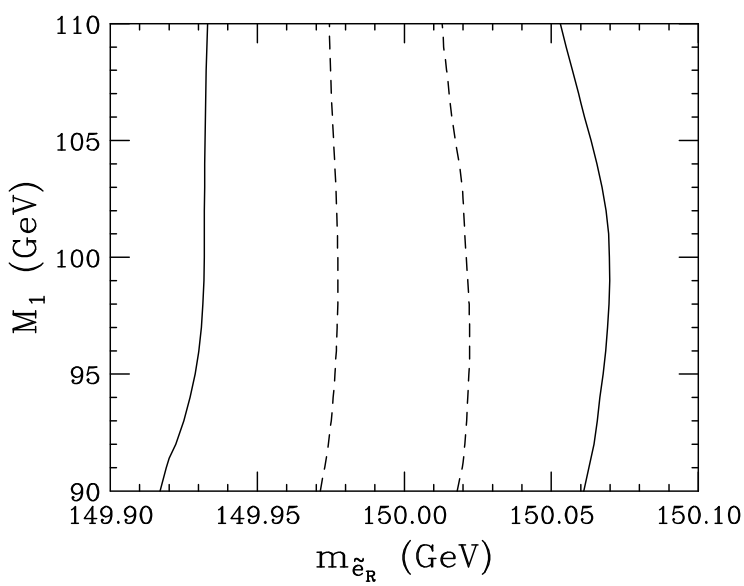

FIG. 8. $\chi^2 = 1$ constraint contours in the $(m_{\tilde{e}_R}, M_1)$ plane for the '$m_{\tilde{e}_R}$-optimized scan' of $\sigma(e^-e^- \to \tilde{e}_R^-\tilde{e}_R^-)$ for $L_{\rm tot} = 1$ fb^{-1} (solid) and 10 fb^{-1} (dashed). The luminosity is concentrated at $E_{\rm CM} = 300$ GeV. $P_{e^-} = 0.8$, and ISR/beamstrahlung, beam energy spread, and the selectron width of Eq. (2) are included.

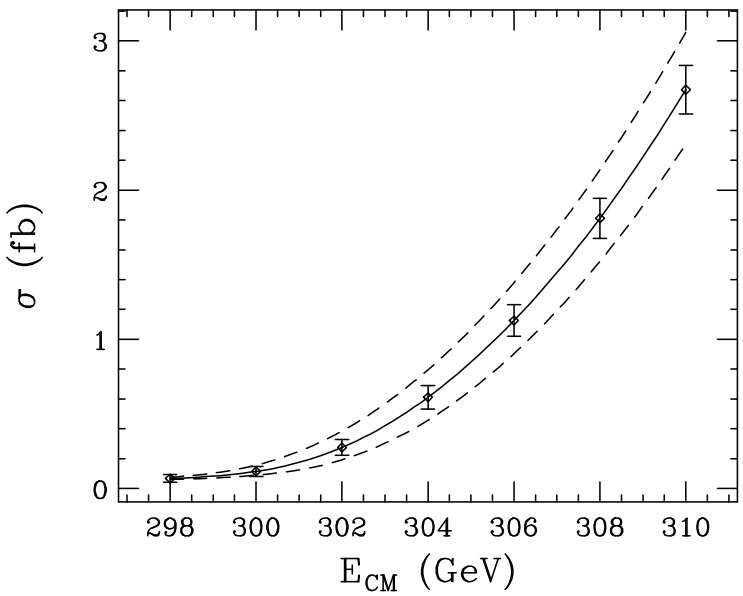

FIG. 9. Threshold behavior for $\sigma(e^+e^- \to \tilde{e}_R^+\tilde{e}_R^-)$ for $(m_{\tilde{e}_R}, m_\chi) = (150\text{ GeV}, 100\text{ GeV})$ (solid) and for $\Delta m_{\tilde{e}_R} = \pm 400$ MeV (dashed). The error bars give the 1σ statistical error corresponding to 100 fb^{-1} per point. $P_{e^-} = 0.8$, $P_{e^+} = 0$, and ISR/beamstrahlung, beam energy spread, and the selectron width are included.

the cuts required to remove them, are necessary to fully understand the potential of e^+e^- threshold studies. In this section we make the most optimistic assumption possible, namely, we neglect all backgrounds. Our conclusion that very large luminosities are required in e^+e^- collisions will only be strengthened with more detailed analyses.

In Figs. 9 and 10 we present threshold cross sections for $\sigma(e^+e^- \to \tilde{e}_R^+\tilde{e}_R^-)$ for $(m_{\tilde{e}_R}, m_\chi) = (150\text{ GeV}, 100\text{ GeV})$, as well as for deviations in $m_{\tilde{e}_R}$ and m_χ. The cross sections are small, and the statistical error bars shown are for 100 fb^{-1} per point, in contrast to the 1 fb^{-1} assumed in Figs. 5 and 6. Note also that, in contrast to the e^-e^- case, deviations in $m_{\tilde{e}_R}$ and M_1 have the same qualitative effect on the threshold curve — roughly speaking, both change the normalization. The effect of increasing $m_{\tilde{e}_R}$ is therefore nearly indistinguishable from the effect of decreasing M_1, and the degeneracy is difficult to remove by threshold scans alone.

As evident in Figs. 9 and 10, data taken at any of the potential scan points provides roughly the same information. We consider a 2-point scan with luminosity divided equally between $E_{\rm CM} = 300$ GeV and 310 GeV; results vary little for different scan strategies. The χ^2 contours are given in Fig. 11. As expected, from threshold data it is very difficult to determine $m_{\tilde{e}_R}$ and M_1 separately. In contrast to the e^-e^- case, one must necessarily rely on kinematic endpoints to break this degeneracy. Assuming the Bino mass is known *exactly*, we find

$$\text{2-point scan: } L_{\rm tot}^{e^+e^-} = 100\ (1000)\ \text{fb}^{-1} \Longrightarrow \Delta m_{\tilde{e}_R} = 210\ (70)\ \text{MeV}\ (1\sigma)\ . \tag{8}$$

If the Bino mass is known only to 1 GeV, these bounds become $L_{\rm tot}^{e^+e^-} = 100\ (1000)$ fb$^{-1} \Longrightarrow \Delta m_{\tilde{e}_R} = 290\ (140)$ MeV (1σ).

Threshold scans in e^+e^- colliders have been studied previously in Refs. [14,15], where measurements of a wide variety of superparticle masses were considered. While our results

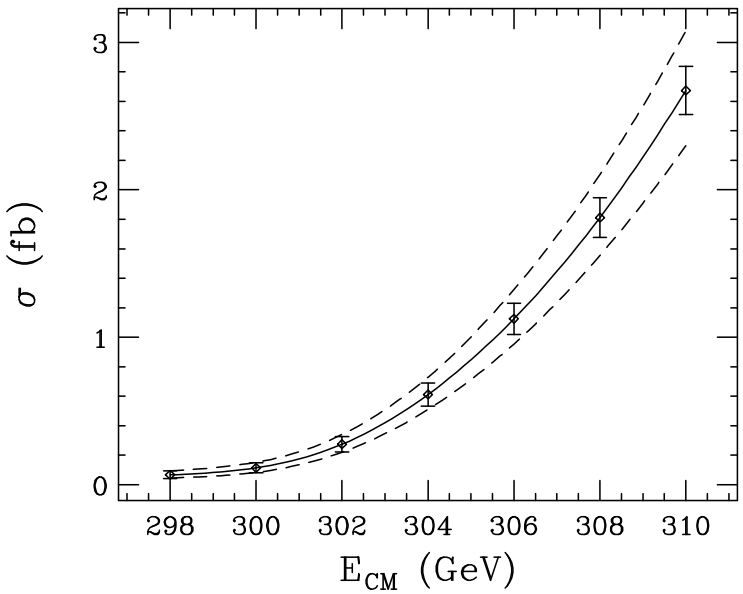

FIG. 10. Threshold behavior for $\sigma(e^+e^- \to \tilde{e}_R^+\tilde{e}_R^-)$ for $(m_{\tilde{e}_R}, m_\chi) = (150\text{ GeV}, 100\text{ GeV})$ (solid) and for $\Delta m_\chi = \pm 4$ GeV (dashed). The error bars give the 1σ statistical error corresponding to 100 fb^{-1} per point. $P_{e^-} = 0.8$, $P_{e^+} = 0$, and ISR/beamstrahlung, beam energy spread, and the selectron width are included.

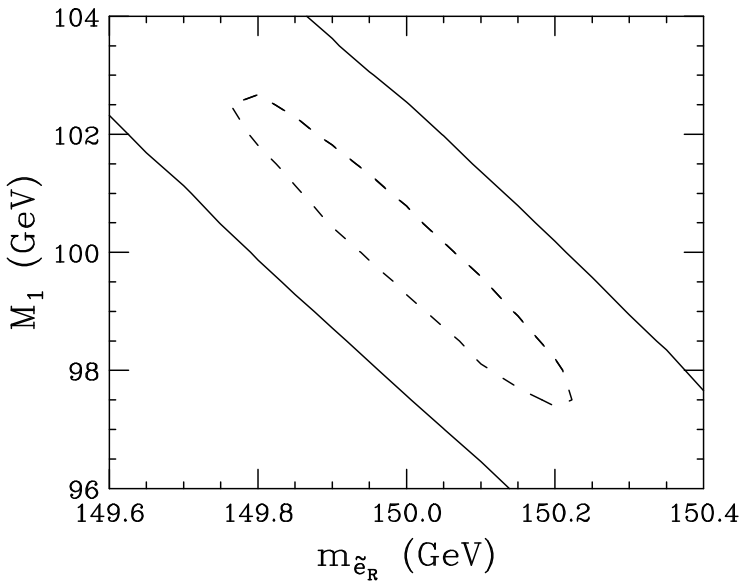

FIG. 11. $\chi^2 = 1$ constraint contours in the $(m_{\tilde{e}_R}, M_1)$ plane for the '2-point scan' of $\sigma(e^+e^- \to \tilde{e}_R^+\tilde{e}_R^-)$ for $L_{\rm tot} = 100$ fb^{-1} (solid) and 1000 fb^{-1} (dashed). The luminosity is divided equally between the points $E_{\rm CM} = 300$ GeV and 310 GeV. $P_{e^-} = 0.8$, $P_{e^+} = 0$, and ISR/beamstrahlung, beam energy spread, and the selectron width are included.

agree qualitatively, we are unable to reproduce their results in detail. In Ref. [14] the authors consider the scenario $(m_{\tilde{e}_R}, m_\chi) = (132\text{ GeV}, 71.9\text{ GeV})$. Assuming $P_{e^-} = 0.8$, $P_{e^+} = 0.6$, and $L_{\rm tot}^{e^+e^-} = 100\text{ fb}^{-1}$ divided equally between the ten points $E_{\rm CM} = 265, 266, \ldots, 274$ GeV, they found $\Delta m_{\tilde{e}_R} = 50$ MeV. With the same assumptions, we find $\Delta m_{\tilde{e}_R} = 90$ MeV (1σ) if M_1 is known exactly, and $\Delta m_{\tilde{e}_R} = 130$ MeV (1σ) if M_1 is known to 1 GeV. Our bounds are significantly less stringent — to achieve $\Delta m_{\tilde{e}_R} = 50$ MeV, we find that at least $L_{\rm tot}^{e^+e^-} = 320\text{ fb}^{-1}$ is required. We stress again that in both analyses, backgrounds are neglected. Once included, the achievable precisions in e^+e^- colliders will certainly deteriorate, possibly significantly.

VI. SUMMARY AND DISCUSSION

The e^-e^- mode is an inexpensive and simple extension of the linear collider program. We have described an important virtue of this mode for studies of supersymmetry, namely, the measurement of selectron mass at threshold. In e^-e^- mode, many potential backgrounds to selectron pair production are simply absent, and those that remain may be suppressed to negligible levels with double beam polarization. In addition, the unique quantum numbers of the e^-e^- initial state lead to large cross sections even slightly above threshold, in contrast to the case of e^+e^- colliders. We have included the ISR/beamstrahlung and beam energy spread of realistic beam designs and find that selectron mass measurements below 100 MeV level are possible with only $L_{\rm tot} = 1\text{ fb}^{-1}$, or less than a week of running at design luminosity. In e^+e^- collisions, such precision, even ignoring large backgrounds, requires more than two orders of magnitude more luminosity.

Throughout this study, we have assumed that the lightest neutralino is a pure Bino, and that slepton flavor violation is absent. It is, of course, important that these assumptions be verifiable experimentally. Note that the results derived here are not dependent on extremely precise cross section measurements. The statistical uncertainties at individual scan points are typically of order 10%, and so the impact of Bino purity and other complications need only be constrained to be below this level.

The neutralino mixing matrix may be constrained most directly by discovering all four neutralinos and two charginos. If they are within kinematic reach of a linear collider, discovery is guaranteed, and their masses and other observables will allow a highly accurate determination of the neutralino mass matrix. Alternatively, if some states, such as the Higgsinos, are beyond reach, observables such as $\sigma(e^+e^-_R \to \chi^+\chi^-)$ [31] may be used to reduce the theoretical uncertainty in $\sigma(e^-e^- \to \tilde{e}^-_R\tilde{e}^-_R)$ to sufficient levels. Slepton flavor violation may also change the prediction for $\sigma(e^-e^- \to e^-e^-\chi\chi)$. However, the resulting signals, such as $\sigma(e^-e^- \to e^-\mu^-\chi\chi)$ are so spectacular that they will be stringently bounded, or, if seen, precisely measured [8]. Such effects, then, will not lead to large theoretical uncertainties. Finally, of course, at loop-level, many unknown supersymmetry parameters enter. However, these are unlikely to disrupt the theoretical calculations of threshold cross sections at the 10% level.

The study described here is but one use of the peculiar features of the $e^-e^- \to \tilde{e}^-_R\tilde{e}^-_R$ reaction. If the lightest supersymmetric particle is Higgsino-like, or in theories with R-parity violation or low-energy supersymmetry breaking, the Bino mass parameter M_1 may be very large. As a result of the Bino mass insertion in Fig. 1, the cross section for $e^-e^- \to \tilde{e}^-_R\tilde{e}^-_R$

is large even for large M_1, and a high precision measurement of M_1 is possible even for $M_1 \sim 1$ TeV [6,32]. In addition, the full arsenal of linear collider modes may allow one to extend the high precision measurement of $m_{\tilde{e}_R}$ to the rest of the first generation sleptons through a series of β threshold scans: $e^-e^- \to \tilde{e}_R^-\tilde{e}_R^-$ yields $m_{\tilde{e}_R}$; $e^+e^- \to \tilde{e}_R^\pm\tilde{e}_L^\mp$ yields $m_{\tilde{e}_L}$; $e^+e^- \to \chi^+\chi^-$ yields $m_{\chi^\pm}$; and $e^-\gamma \to \tilde{\nu}_e\chi^-$ yields $m_{\tilde{\nu}_e}$ [33]. The quantity $m_{\tilde{e}_L} - m_{\tilde{e}_R}$ gives a highly model-independent measurement of $\tan\beta$ [6]. More generally, as noted previously, precise measurements of all of these masses will play an essential role in the program of extrapolating weak scale parameters to higher energy scales to uncover a more fundamental theory of nature.

ACKNOWLEDGMENTS

We thank Claus Blöchinger and Kathy Thompson for helpful conversations and Clemens Heusch for encouragement. The work of JLF was supported in part by the U. S. Department of Energy under cooperative research agreement DF–FC02–94ER40818. The work of MEP was supported by the Department of Energy, contract DE–AC03–76SF00515.

REFERENCES

[1] H. Murayama and M. E. Peskin, Ann. Rev. Nucl. Part. Sci. **46**, 533 (1996) [hep-ex/9606003].

[2] *Proceedings of the 1st International Workshop on Electron-Electron Interactions at TeV Energies (e^-e^-95)*, Santa Cruz, California, 5–6 September 1995, ed. C. A. Heusch, Int. J. Mod. Phys. A **11**, 1523-1697 (1996).

[3] *Proceedings of the 2nd International Workshop on Electron-Electron Interactions at TeV Energies (e^-e^-97)*, Santa Cruz, California, 22–24 September 1997, ed. C. A. Heusch, Int. J. Mod. Phys. A **13**, 2217-2549 (1998).

[4] *Proceedings of the 3nd International Workshop on Electron-Electron Interactions at TeV Energies (e^-e^-99)*, Santa Cruz, California, 10–12 December 1999, ed. C. A. Heusch, Int. J. Mod. Phys. A **15**, 2347-2628 (2000).

[5] W. Y. Keung and L. Littenberg, Phys. Rev. D **28**, 1067 (1983).

[6] J. L. Feng, Int. J. Mod. Phys. A **13**, 2319 (1998) [hep-ph/9803319].

[7] J. L. Feng, Int. J. Mod. Phys. A **15**, 2355 (2000) [hep-ph/0002055].

[8] N. Arkani-Hamed, H. Cheng, J. L. Feng and L. J. Hall, Phys. Rev. Lett. **77**, 1937 (1996) [hep-ph/9603431].

[9] N. Arkani-Hamed, J. L. Feng, L. J. Hall and H. Cheng, Nucl. Phys. B **505**, 3 (1997) [hep-ph/9704205].

[10] H. Cheng, J. L. Feng and N. Polonsky, Phys. Rev. D **56**, 6875 (1997) [hep-ph/9706438]; Phys. Rev. D **57**, 152 (1998) [hep-ph/9706476].

[11] H. Cheng, Int. J. Mod. Phys. A **13**, 2329 (1998) [hep-ph/9801234].

[12] G. A. Blair, W. Porod and P. M. Zerwas, Phys. Rev. D **63**, 017703 (2001) [hep-ph/0007107].

[13] M. E. Peskin, `pandora 2.1`, http://www-sldnt.slac.stanford.edu/nld/new/Docs/Generators/PANDORA.htm.

[14] H. Martyn and G. A. Blair, hep-ph/9910416.

[15] H. U. Martyn, hep-ph/0002290.

[16] M. E. Peskin, Int. J. Mod. Phys. A **13**, 2299 (1998) [hep-ph/9803279].

[17] M. Skrzypek and S. Jadach, Z. Phys. C **49**, 577 (1991).

[18] M. E. Peskin, Linear Collider Collaboration technical note LCC–0010 (1999).

[19] K. Yokoya and P. Chen, in *Proceedings of the 1989 Particle Accelerator Conference*, eds. F. Bennett and L. Taylor (IEEE, 1989).

[20] P. Chen, Phys. Rev. D **46**, 1186 (1992).

[21] P. Chen, T. L. Barklow and M. E. Peskin, Phys. Rev. D **49**, 3209 (1994) [hep-ph/9305247].

[22] K. A. Thompson and P. Chen, in *Physics and Experiments at Future Linear e^+e^- Colliders* (LCWS99), eds. E. Fernandez and A. Pacheco (U. Auton. de Barcelona, Bellaterra, 2000).

[23] K. A. Thompson, Int. J. Mod. Phys. A **15**, 2485 (2000).

[24] T. Raubenheimer, private communication.

[25] T. Raubenheimer, talk presented at the 5th International Linear Collider Workshop, Fermilab, 24-28 October 2000.

[26] F. Zimmermann, K. A. Thompson and R. H. Helm, Int. J. Mod. Phys. A **13**, 2443 (1998).

[27] F. Cuypers, G. J. van Oldenborgh and R. Rückl, Nucl. Phys. B **409**, 128 (1993) [hep-ph/9305287].
[28] F. Cuypers, K. Kolodziej and R. Rückl, Nucl. Phys. B **430**, 231 (1994) [hep-ph/9405421].
[29] D. Choudhury and F. Cuypers, Nucl. Phys. B **429**, 33 (1994) [hep-ph/9405212].
[30] G. W. Wilson, in *Physics and Experiments at Future Linear e^+e^- Colliders* (LCWS99), eds. E. Fernandez and A. Pacheco (U. Auton. de Barcelona, Bellaterra, 2000).
[31] J. L. Feng, M. E. Peskin, H. Murayama and X. Tata, Phys. Rev. D **52**, 1418 (1995) [hep-ph/9502260].
[32] C. Blöchinger, H. Fraas, T. Mayer and G. Moortgat-Pick, hep-ph/0101176.
[33] V. Barger, T. Han and J. Kelly, Phys. Lett. B **419**, 233 (1998) [hep-ph/9709366].